Hindawi
Mathematical Problems in Engineering
Volume 2020, Article ID 8258507, 13 pages
https://doi.org/10.1155/2020/8258507

Research Article

Analysis of a Novel Two-Lane Hydrodynamic Lattice Model Accounting for Driver's Aggressive Effect and Flow Difference Integral

Xinyue Qi[1,2,3] **Hongxia Ge**[1,2,3] **and Rongjun Cheng**[1,2,3]

[1]*Faculty of Maritime and Transportation, Ningbo University, Ningbo 315211, China*
[2]*Jiangsu Province Collaborative Innovation Center for Modern Urban Traffic Technologies, Nanjing 210096, China*
[3]*National Traffic Management Engineering and Technology Research Centre Ningbo University Sub-Centre, Ningbo 315211, China*

Correspondence should be addressed to Rongjun Cheng; chengrongjun76@126.com

Received 15 April 2020; Accepted 15 May 2020; Published 30 May 2020

Guest Editor: Miaojuan Peng

In the actual traffic environment, the driver's aggressive driving behaviors are closely related to the traffic conditions at the next-nearest grid point at next time step. The driver adjusts the acceleration of the driving vehicle by predicting the density of the front grid points. Considering the driver's aggressive effect and the relative flow difference integral, a novel two-lane lattice hydrodynamic model is presented in this paper. The linear stability method is used to analyze the current stability of the new model, and the neutral stability curve is obtained. The nonlinear analysis of the new model is carried out by using the theory of perturbations, and the mKdV equation describing the density of the blocked area is derived. The theoretical analysis results are verified by numerical simulation. From the analysis results, it can be seen that the driver's aggressive effect and the relative flow difference integral can improve the stability of traffic flow comprehensively.

1. Introduction

The rapid improvement of urbanization level and the explosive growth of household car ownership have made urban traffic contradiction more and more prominent and even become an important factor restricting urban economic development. Especially since 1990, it is the fastest growing period of motor vehicles. The traffic flow is more concentrated, unable to move and stop, and the contradiction is extremely sharp. In order to change the traffic situation, many big cities began to construct ring roads, large interchanges, elevated roads, and metro. Because of the hasty decision and improper decision-making, they often only pay attention to local improvement and can only achieve short-term results. If the city is compared to the human body, then traffic is equivalent to the flow of human blood. The flow of blood is not smooth, accidents occur frequently, the light cause is short-term paralysis, and the heavy cause is long-term poor flow and the formation of "dead city," which will bring immeasurable losses to the country and people. Traffic flow theory comes into being under such circumstances. Furthermore, some researchers [1–3] have broadened the field of traffic flow research from other perspectives in recent years.

In the face of many hazards brought by traffic congestion, the construction and development of urban roads urgently need the support and guidance of theoretical knowledge, and the theoretical model of traffic flow is applied. In order to explore the intrinsic mechanism of traffic congestion, scholars at home and abroad have carried out a series of studies on the physical phenomena of traffic flow [4–28]. Based on the characteristics of traffic flow, various traffic models have been developed through research, such as car-following models [26, 29–35], cellular automata models [36–41], macro-traffic models [42–47], and lattice hydrodynamic model [30, 48–52].

Lattice hydrodynamic modeling and nonlinear analysis are important tools for macro-traffic flow simulation and traffic pressure relief. Lattice hydrodynamics model has been widely used to simulate the phase transition phenomena in real traffic because it can describe the macroscopic characteristics of traffic flow. Nagatani [12, 13] discretized the hydrodynamic model to obtain a simple lattice hydrodynamic model, which incorporated the optimized velocity function of the micromodel into the macromodel. Therefore, the lattice hydrodynamic model has both the characteristics of macromodel and micromodel, and it is convenient for simulation calculation and prediction. Based on the lattice hydrodynamic model of Nagatani [13], many extended models are proposed to study the nonlinear phenomena in traffic flow under intelligent transportation environment. Xue [14] established a one-dimensional traffic flow lattice hydrodynamic model considering the interaction between the nearest neighbor and the next-nearest neighbor lattices. Using the linear stability theory, they deduced the neutral stability conditions of traffic flow and the mKdV equation describing the phase transition of traffic congestion by using the nonlinear analysis method. Considering the influence of any number of lattice information in front, Ge et al. [15] proposed an extended lattice hydrodynamic model. Ge and Cheng [16] further improved the lattice model by combining "backward looking" effect and deduced the mKdV equation near the neutral stable line. Considering the optimal traffic flow, Zhu et al. [17, 18] extended the lattice model and found that this model can significantly alleviate traffic congestion. On the basis of previous studies, Peng et al. [19, 20] combined various road information to further promote the study of lattice hydrodynamics model. Tian et al. [21, 22] considered different traffic information to further improve and apply the lattice hydrodynamic model of Nagatani.

Using lane changing rules, Nagatani [53] constructed a new extended two-lane traffic model with $v_{\max} = 1$. In recent years, two-lane traffic flow models [54–66] have been developed gradually due to the restrictions of single lane being unable to change lanes and overtaking. In these two-lane traffic flow models, more attention is paid to the relative displacement, speed between two adjacent vehicles. However, in the real traffic flow, the driver's aggressive driving behaviors also have a significant impact on the traffic situation. In real traffic life, the aggressive driving behaviors are closely related to the starting, braking, overtaking, and lane changing of driving vehicle. At the same time, the integral form of flow difference can describe traffic flow more accurately and objectively. In the two-lane lattice hydrodynamic model, a new model is proposed with consideration of driver's aggressive effect and flow difference integral.

This paper consists of the following parts. Firstly, the development history of traffic flow related models is introduced in Section 1. Based on the existing models, an extended two-lane lattice hydrodynamic model is proposed in Section 2. In Section 3, the linear stability analysis of the new model is presented. In Section 4, the new model is analyzed by nonlinear analysis method and the mKdV equation is solved. Numerical simulations are carried out in Section 5. Finally, the conclusions are provided in Section 6.

2. The Novel Two-Lane Lattice Hydrodynamic Model

With the rapid development of the modern urban process, the situation of single lane in the real road environment is gradually reduced, which makes the study of single lane traffic model cannot meet the needs of the actual road traffic. This contradiction has gradually attracted the attention of traffic flow researchers, and the two-lane traffic model came into being. Compared with single lane, the two-lane traffic model can reflect the complexity of the actual traffic, and more and more academic papers on the two-lane model gradually increase. But at present, the research of the two-lane model has a lot of room to expand, which is the significance of this paper. Figure 1 shows the diagrammatic sketch of the lane change in a two-lane expressway traffic flow model, in which continuous two-lane traffic flow is discretized into two rows of uniform grid points.

The direction of the arrow shown in Figure 1 represents the forward flow direction of traffic flow in actual traffic operation, and each circle represents a grid point. When the traffic flow gap between two rows at a grid point is too large, the traffic flow will be adjusted according to the actual situation: part of the traffic flow will be transferred from the large part to the small part of the traffic flow. As shown in Figure 1, when the traffic flow in site $j-1$ of the second lane is larger than that in site j of the first lane, a large part of the traffic flow flows from point $j-1$ of the second lane to point j of the first lane. If the traffic flow in point j of the first lane is larger than that in point $j+1$ of the second lane, some traffic flow will be transferred from point j to point $j+1$. In the course of lane changing of two-lane traffic flow, we define lane changing rate as $\gamma|\rho_0^2 V'(\rho_0)|$, with dimensionless constant coefficient represented by γ.

In the absence of lane diversion, the conservation equation of the site j on the first lane is given as

$$\begin{aligned}&\partial_t \rho_{1,j} + \rho_0\left(\rho_{1,j}v_{1,j} - \rho_{1,j-1}v_{1,j-1}\right)\\&\quad = \gamma|\rho_0^2 V'(\rho_0)|\left(\rho_{2,j-1} - 2\rho_{1,j} + \rho_{2,j+1}\right),\end{aligned} \tag{1}$$

and the conservation equation of the site j on the second lane is given as

$$\begin{aligned}&\partial_t \rho_{2,j} + \rho_0\left(\rho_{2,j}v_{2,j} - \rho_{2,j-1}v_{2,j-1}\right)\\&\quad = \gamma|\rho_0^2 V'(\rho_0)|\left(\rho_{1,j-1} - 2\rho_{2,j} + \rho_{1,j+1}\right),\end{aligned} \tag{2}$$

where $\rho_{1,j}$ and $\rho_{2,j}$ denote the density of the lattice j on the first lane and the second lane, respectively. $\rho_{1,j}v_{1,j} - \rho_{1,j-1}v_{1,j-1}$ represents the relative flux difference between the lattices j and $j-1$ of the first lane. $\rho_{2,j}v_{2,j} - \rho_{2,j-1}v_{2,j-1}$ represents the relative flux difference between the lattices j and $j-1$ of the second lane.

By substituting equation (1) into equation (2), the two-lane continuity equation is obtained as follows:

$$\partial_t \rho_j + \rho_0\left(\rho_j v_j - \rho_{j-1}v_{j-1}\right) = \gamma|\rho_0^2 V'(\rho_0)|\left(\rho_{j-1} - 2\rho_j + \rho_{j+1}\right), \tag{3}$$

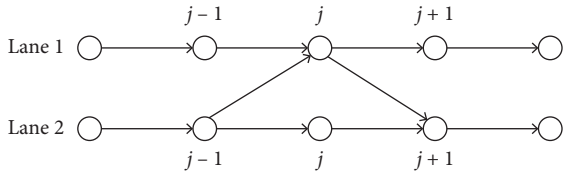

Figure 1: The schematic model of traffic flow on a two-lane highway.

where ρ_0 is the initial density, $\rho_j = ((\rho_{1,j} + \rho_{2,j})/2)$ and $\rho_j v_j = ((\rho_{1,j} v_{1,j} + \rho_{2,j} v_{1,j})/2)$.

Assuming that the evolution equation of traffic flow on each lane is not affected by the lane change proposed by Nagatani, the evolution equation of two-lane traffic is as follows:

$$\partial_t\left(\rho_j v_j\right) = a\rho_0 V\left(\rho_{j+1}\right) - a\rho_j v_j, \tag{4}$$

where driver's sensitivity coefficient is defined as a, and $a = (1/\tau)$. $V(\rho_{j+1})$ in equation (4) represents the optimal velocity function, and $V(\rho_{j+1}) = ((V(\rho_{1,j+1}) + V(\rho_{2,j+1}))/2)$.

The optimal velocity function is adopted as follows:

$$V(\rho) = \frac{v_{\max}}{2}\left[\tanh\left(\frac{2}{\rho_0} - \frac{\rho}{\rho_0^2} - \frac{1}{\rho_c}\right) + \tanh\left(\frac{1}{\rho_c}\right)\right], \tag{5}$$

where $v_{\max} = 2$ is the maximal velocity and $\rho_c = 4$ is the safety density.

A large number of studies have shown that driver's habits and personality will affect traffic flow in varying degrees. However, at this stage, no scholars have taken the driver's aggressive effect into account in two-lane traffic. Based on this, we take the driver's aggressive driving behaviors into two-lane to explore what the specific impact of driver's aggressive effect will have on two-lane traffic operation. We use the integral form of flow difference to give the specific density of the current road. To sum up, a new extended two-lane model of traffic flow is constructed, and its continuity equation and the motion equation are listed as follows:

$$\begin{aligned}\partial_t\left(\rho_j v_j\right) = {} & a\rho_0\left[(1-P)V\left(\rho_{j+1}(t)\right) + PV\left(\rho_{j+2}(t+t_0)\right)\right] \\ & - a\rho_j v_j + a\beta\int_{t-t_0}^{t}\left[\rho_{j+1}(s)v_{j+1}(s) - \rho_j(s)v_j(s)\right]\mathrm{d}s,\end{aligned} \tag{6}$$

$$\partial_t\rho_j + \rho_0\left(\rho_j v_j - \rho_{j-1}v_{j-1}\right) = \gamma\left|\rho_0^2 V'(\rho_0)\right|\left(\rho_{j-1} - 2\rho_j + \rho_{j+1}\right), \tag{7}$$

where $\int_{t-t_0}^{t}[\rho_{j+1}(s)v_{j+1}(s) - \rho_j(s)v_j(s)]$ represents the integral of the flow difference between $t - t_0$ and t, besides, gives the integral a coefficient β. In actual traffic, compared with ordinary drivers, some drivers who are confident of their driving skills will drive vehicles close to their front because they can quickly predict the driving information of the front car, adjust, and accelerate in time. P is the weighting value, $0 \le P \le 0.5$, which means the intensity of the driver's aggressive effect. As $P = 0$, this new expanded traffic model returns to Nagatani's model [13].

The dynamic equation of traffic density can be obtained by eliminating the velocity v in equations (6) and (7). The equation is expressed as follows:

$$\begin{aligned}& a\rho_0^2\left[(1-P)\left(V\left(\rho_{j+1}(t)\right) - V\left(\rho_j(t)\right)\right) + P\left(V\left(\rho_{j+2}(t+t_0)\right)\right.\right. \\ & \left.\left. - V\left(\rho_{j+1}(t+t_0)\right)\right)\right] \\ & + \partial_t^2\rho_j(t) - \gamma\left|\rho_0^2 V'(\rho_0)\right|\left(\partial_t\rho_{j-1} - 2\partial_t\rho_j + \partial_t\rho_{j+1}\right) + a\,\partial_t\rho_j \\ & - a\gamma\left|\rho_0^2 V'(\rho_0)\right|\left(\rho_{j-1}(s) - 2\rho_j(s) + \rho_{j+1}(s)\right) \\ & - a\beta\left[\rho_{j+1}(t) - \rho_{j+1}(t-t_0) - \rho_j(t) + \rho_j(t-t_0)\right] \\ & + a\beta\tau\gamma\left|\rho_0^2 V'(\rho_0)\right|\sum_{l=1}^{L}\left(3\rho_j(t-l\tau) - 3\rho_{j+1}(t-l\tau)\right. \\ & \left. + \rho_{j+2}(t-l\tau) - \rho_{j-1}(t-l\tau)\right) = 0.\end{aligned} \tag{8}$$

3. Linear Stability Analysis

In this section, linear analysis is used to discuss the driver's aggressive effect, the relative flow difference integral, and the lane change rate on traffic operation. Obviously, the uniform traffic flow means constant density ρ_0 and constant velocity $V(\rho)$, so the steady-state solution of the traffic flow for this new model is given as follows:

$$\begin{aligned}\rho_j(t) &= \rho_0, \\ v_j(t) &= V(\rho),\end{aligned} \tag{9}$$

y_j is assumed to be a small disturbance of steady-state flow on lattice j, and let

$$\rho_j(t) = \rho_0 + y_j(t). \tag{10}$$

Inserting equation (10) into equation (8), one obtains

$$\begin{aligned}& \partial_t^2 y_j + a\partial_t y_j - a\beta\left[y_{j+1} - y_{j+1}(t-t_0) - y_j + y_j(t-t_0)\right] \\ & + a\rho_0^2 PV'(\rho_0)\left(y_{j+2} - y_{j+1}\right) + a\rho_0^2 PV'(\rho_0)t_0\left(\partial_t y_{j+2} - \partial_t y_{j+1}\right) \\ & + a\gamma\rho_0^2 V'(\rho_0)\left(y_{j-1} - 2y_j + y_{j+1}\right) + a\gamma\rho_0^2 V'(\rho_0)\left(y_{j-1} - 2y_j + y_{j+1}\right) \\ & + a\rho_0^2(1-P)V'(\rho_0)\left(y_{j+1} - y_j\right) + \gamma\rho_0^2 V'(\rho_0)\left[\partial_t y_{j-1} - 2\partial_t y_j + \partial_t y_{j+1}\right] \\ & - a\beta\gamma\rho_0^2 V'(\rho_0)\tau\sum_{l=1}^{L}\left[3y_j(t-l\tau) - 3y_{j+1}(t-l\tau) + y_{j+2}(t-l\tau) - y_{j-1}(t-l\tau)\right] = 0.\end{aligned} \tag{11}$$

The following equation about z is derived by expanding $y_j = \exp(ikj + zt)$:

$$\begin{aligned} & a\rho_0^2\left[(1-P)V'(\rho_0)\left(e^{ik}-1\right)+PV'(\rho_0)\left(e^{2ik}-e^{ik}\right)\right. \\ & \left.+Pt_0V'(\rho_0)z\left(e^{2ik}-e^{ik}\right)\right] \\ & +a\gamma\rho_0^2V'(\rho_0)\left(e^{-ik}-2+e^{ik}\right)-a\beta\left(e^{ik}-e^{ik-zt_0}-1+e^{-zt_0}\right) \\ & +z^2+az+\gamma\rho_0^2V'(\rho_0)z\left(e^{-ik}-2+e^{ik}\right) \\ & -a\beta\tau\gamma\rho_0^2V'(\rho_0)\sum_{l=1}^{L}e^{-lz\tau}\left(3-3e^{ik}+e^{2ik}-e^{-ik}\right)=0, \end{aligned} \tag{12}$$

where $V'(\rho_0) = (\mathrm{d}V(\rho)/\mathrm{d}\rho)|\rho = \rho_0$, and the sum $\sum_{l=1}^{L} e^{-lz\tau}$ can be expressed as $\sum_{l=1}^{L} e^{-lz\tau} = L$. Let $z = z_1(ik) + z_2(ik)^2 + \cdots$, in the equation, omit the higher order terms of ik larger than the second power, we obtain

$$z_1 = -\rho_0^2V'(\rho_0), \tag{13}$$

$$z_2 = -\frac{\left[\rho_0^2V'(\rho_0)\right]^2}{a}-\rho_0^2V'(\rho_0)\left[\frac{1}{2}-P-Pt_0z_1-\gamma\right]+\beta t_0z_1. \tag{14}$$

When the value of z_2 is less than 0, the uniform steady-state flow will be unstable for long-wavelength modes. In contrast, when the value of z_2 is greater than 0, the uniform steady-state flow will remain stable. After introducing equation (13) into equation (14), we get the neutral stability condition is as follows:

$$a = -\frac{2\rho_0^2V'(\rho_0)}{1-P-Pt_0z_1-\gamma+\beta t_0}. \tag{15}$$

The stable region of two-lane traffic flow system can be obtained by satisfying the following condition:

$$a > -\frac{2\rho_0^2V'(\rho_0)}{1-P-Pt_0z_1-\gamma+\beta t_0}. \tag{16}$$

Figure 2 reveals the phase diagram in the (ρ, a)-plane. With the change of the influence coefficient of different parameters, the correlation between the variation and parameters of the stable and unstable regions can be shown in Figure 2.

In Figure 2, the solid and dotted lines of color represent the neutral stability curves presented under different constraints. Figure 2(a) shows the neutral stability curves of three color dotted lines when $P = 0.1$, $\gamma = 0$ and β values are changed to 0, 0.05, and0.1, respectively. The three solid lines represent the neutral stability curves when $P = 0.1$, $\gamma = 0$ and β is changed to 0, 0.05, and 0.1. Among them, the unstable region is shown below the curve and the stable region is shown above the curve. By comparing dotted lines separately, we can see that the value of β increases gradually, the area of unstable region decreases gradually, and the surface value of stable region increases gradually. Similarly, by comparing the three solid lines in the graph, we deduce that when $P = 0.1$ and $\gamma = 0.1$, changing the value of β, the value of neutral stability curve decreases gradually, and the area of unstable region decreases accordingly. The two lines with the same color are the neutral stability curves when the values of P and β are fixed and the values of γ are 0 and 0.1, respectively. By comparing each solid line with the dashed line, we find that when $\gamma = 0.1$, the neutral stability curve is below the neutral stability curve when $\gamma = 0$. It can be explained that increasing the lane change rate γ has a stabilizing effect on traffic flow.

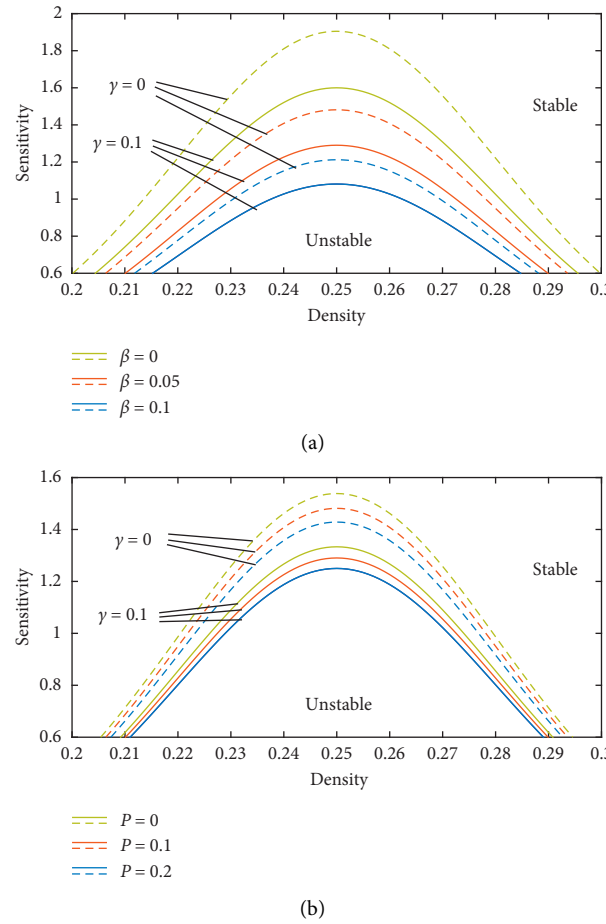

Figure 2: Phase diagram in parameter space (ρ, a) for equation (16). (a) $P = 0.1$. (b) $\beta = 0.05$.

Figure 2(b) shows the neutral stability curve when the density difference integral β is 0.05 and P is 0, 0.1, and 0.2, respectively. Three color dotted lines are neutral stability curves with $\gamma = 0$, and three color solid lines are neutral stability curves with $\gamma = 0.1$. It is obvious that increasing the value of P can gradually expand the stability region by changing the curve in the graph. Similarly, when comparing $\gamma = 0$ and $\gamma = 0.1$, respectively, the two curves with the same γ value can be seen that when γ takes 0.1, the stability region is larger. We can conclude that increasing lane change rate γ is beneficial to traffic flow stability in a certain range. Through the current stability analysis, we can get the neutral stability curve, and the simulation results can be verified. Finally, it is concluded that increasing the values of the driver's aggressive effect, the relative flow difference integral, and the lane change rate is helpful to relieve traffic pressure.

4. The mKdV Equation

In this section, the reduced perturbation method is used to analyze the above model near the critical point (ρ_c, a_c). In the unstable area of traffic flow, the slow variables X and T for a small direct scaling parameter $\varepsilon(0 < \varepsilon \ll 1)$ are supposed as follows:

$$\begin{aligned} X &= \varepsilon(j + bt), \\ T &= \varepsilon^3 t, \end{aligned} \tag{17}$$

where b alleges a constant to be determined.

The density is defined as follows:

$$\rho_j(t) = \rho_c + \varepsilon R(X, T). \tag{18}$$

By introducing equations (17) and (18) into equation (8), the following nonlinear partial differential expression is obtained:

$$\begin{aligned} &\varepsilon^2\left(h_1\partial_X R\right) + \varepsilon^3 h_2 \partial_X^2 R + \varepsilon^4\left(\partial_T R + h_3\partial_X^3 R + h_4\partial_X R^3\right) \\ &\quad + \varepsilon^5\left(h_5\partial_X\partial_T R + h_6\partial_X^4 R + h_7\partial_X^2 R^3\right) = 0, \end{aligned} \tag{19}$$

where the coefficients values $h_i(i = 1, 2, \ldots, 7)$ contained in equation (19) are given by

$$\begin{aligned} h_1 &= b + \rho_c^2 V'(\rho_0), \\ h_2 &= \frac{b^2}{a} + \frac{\rho_c^2 V'(\rho_0)}{2} + Pb + \gamma\rho_c^2 V'(\rho_0) + \beta\tau L, \\ h_3 &= \frac{\gamma b\rho_c^2 V'(\rho_0)}{a} + \frac{\rho_c^2 V'(\rho_0)}{6} - \beta b\tau^2 \sum_{l=1}^{L} l + \frac{Pb}{2} - P\gamma\rho_c^2 V'(\rho_0) \\ h_4 &= \frac{\rho_c^2 V'''(\rho_0)}{6}, \\ h_5 &= \frac{2b}{a} - P, \\ h_6 &= \frac{\rho_c^2 V'(\rho_0)}{24} + \frac{\gamma\rho_c^2 V'(\rho_0)}{12} + \frac{\beta b^2\tau^3}{2} \sum_{l=1}^{L} l^2 + \frac{\beta\tau L}{12} - \frac{Pb}{6} \\ &\quad - \frac{P\gamma\rho_c^2 V'(\rho_0)}{2}, \\ h_7 &= \frac{\rho_c^2 V'''(\rho_0)}{12}, \end{aligned} \tag{20}$$

where $V' = (\mathrm{d}V(\rho)/\mathrm{d}\rho)|\rho = \rho_c$ and $V''' = (\mathrm{d}^3 V(\rho)/\mathrm{d}\rho^3)|\rho = \rho_c$.

By substituting $b = -\rho_c^2 V'(\rho_c)$, $\tau = (1 + \varepsilon^2)\tau_c$ into equation (19), the simplified equation is obtained as follows:

$$\varepsilon^4\left(\partial_T R - g_1\partial_X^3 R + g_2\partial_X R^3\right) + \varepsilon^5\left(g_3\partial_X^2 R + g_4\partial_X^4 R + g_5\partial_X^2 R^3\right) = 0, \tag{21}$$

where the parameter values $g_i(i = 1, 2, \ldots, 5)$ in equation (21) are given by

$$\begin{aligned} g_1 &= -\frac{b\gamma\rho_c^2 V'(\rho_0)}{a_c} - \frac{\rho_c^2 V'(\rho_0)}{6} + \beta b\tau^2 \sum_{l=1}^{L} l + \frac{Pb}{2} + P\gamma\rho_c^2 V'(\rho_0), \\ g_2 &= \frac{\rho_c^2 V'''(\rho_0)}{6}, \\ g_3 &= -\frac{\rho_c^2 V'(\rho_0)}{2} - P\rho_c^2 V'(\rho_0) - \gamma\rho_c^2 V'(\rho_0) + \beta\tau L, \\ g_4 &= \frac{\gamma\rho_c^2 V'(\rho_0)}{12} + \frac{\rho_c^2 V'(\rho_0)}{24} + \frac{1}{2}\beta b^2\tau^3 \sum_{l=1}^{L} l^2 + \frac{\beta\tau L}{12} - \frac{Pb}{6} \\ &\quad - \frac{P\gamma\rho_c^2 V'(\rho_0)}{2} \\ &\quad - \left(\frac{2b}{a_c} - P\right) \times \left(\frac{\gamma b\rho_c^2 V'(\rho_0)}{a_c} + \frac{\rho_c^2 V'(\rho_0)}{6} - \beta b\tau^2 \sum_{l=1}^{L} l \right. \\ &\quad \left. + \frac{Pb}{2} - P\gamma\rho_c^2 V'(\rho_0)\right), \\ g_5 &= \frac{\rho_c^2 V'''}{12} - \frac{\rho_c^2 V'''}{6} \times \left(\frac{2b}{a_c} - P\right). \end{aligned} \tag{22}$$

In order to derive the regularization equation, the following transformations should be made:

$$\begin{aligned} T &= \frac{1}{g_1} T', \\ R &= \sqrt{\frac{g_1}{g_2}} R'. \end{aligned} \tag{23}$$

It is drawn out that the mKdV equation with an $O(\varepsilon)$ correction term is given as follows:

$$\partial_T R' = \partial_X^3 R' - \partial_X R'^3 + \varepsilon M[R_0'], \tag{24}$$

where $M[R_0'] = (g_3/g_1)\partial_X^2 R' + (g_4/g_1)\partial_X^4 R' + (g_1 g_5/g_2)\partial_X^2 R'^3$. Subsequently, when ignoring the $O(\varepsilon)$, the kink-antikink soliton solutions of the mKdV equation are proved as follows:

$$R_0'(X, T') = \sqrt{c}\tanh\sqrt{\frac{c}{2}}(X - cT'), \tag{25}$$

where c means the determined velocity of the kink-antikink solution. By solving the following integral equation, the value of c will be obtained:

$$\begin{aligned} &\int_{-\infty}^{+\infty} \frac{\sqrt{c}}{g_1 g_2}\left(g_2 g_3\partial_X^2 R' + g_2 g_4\partial_X^4 R' + g_1 g_5\partial_X^2 R'^3\right) \\ &\quad \tanh\left(\sqrt{\frac{c}{2}}\left(X - cT'\right)\right)\mathrm{d}X = 0. \end{aligned} \tag{26}$$

Suppose $R'(X, T') = R_0'(X, T') + \varepsilon R_1'(X, T')$ takes account of $O(\varepsilon)$ correction. Among them, $(R_0', M[R_0'] \equiv \int_{-\infty}^{+\infty} \mathrm{d}X' R_0' M[R_0'])$. With the method

described in Ref. [48], the general velocity c is obtained as follows:

$$c = \frac{5g_2g_3}{2g_2g_4 - 3g_1g_5}. \tag{27}$$

Therefore, the kink-antikink solution of the mKdV equation near the critical point can be rewritten as follows:

$$\rho_j(t) = h_c \pm \sqrt{\frac{g_1 c}{g_2}\left(\frac{\tau}{\tau_c} - 1\right)} \times \tanh\sqrt{\frac{c}{2}\left(\frac{\tau}{\tau_c} - 1\right)} \times \left[j + (1 - cg_1)\left(\frac{\tau}{\tau_c} - 1\right)t\right]. \tag{28}$$

5. Numerical Simulation

In this section, the influence of the driver's aggressive driving behaviors and the relative flow difference integral of traffic flow are verified by numerical simulation [64–66]. In order to facilitate numerical simulation, equation (8) is simplified by using difference method as follows:

$$\begin{aligned}
&a\beta\tau^2\frac{L(L+1)}{2}\Delta t\left[\rho_{j+1}(t+\Delta t) - \rho_{j+1}(t) - 2\rho_j(t+\Delta t) + 2\rho_j(t) + \rho_{j-1}(t+\Delta t) - \rho_{j-1}(t)\right] \\
&- \gamma\rho_0^2V'(\rho_0)\Delta t\left[\rho_{j-1}(t+\Delta t) - \rho_{j-1}(t) - 2\rho_j(t+\Delta t) + 2\rho_j(t) + \rho_{j+1}(t+\Delta t) - \rho_{j+1}(t)\right] \\
&- \rho_j(t+2\Delta t) + 2\rho_j(t+\Delta t) - \rho_j(t) - a\beta\tau L\Delta t^2\left[\rho_{j+1}(t) - 2\rho_j(t) + \rho_{j-1}(t)\right] \\
&- a\gamma\rho_0^2V'(\rho_0)\Delta t^2\left[\rho_{j-1}(t) - 2\rho_j(t) + \rho_{j+1}(t)\right] \\
&+ aP\Delta t\left[\rho_{j+1}(t+\Delta t) - \rho_{j+1}(t) - \rho_j(t+\Delta t) + \rho_j(t)\right] \\
&- a\rho_0^2\left[V\left(\rho_{j+1}(t)\right) - V\left(\rho_j(t)\right)\right] - a\Delta t\left[\rho_j(t+\Delta t) - \rho_j(t)\right] \\
&+ aP\gamma\rho_0^2V'(\rho_0)\Delta t^2\left[3\rho_j(t) - 3\rho_{j+1}(t) + \rho_{j+2}(t) - \rho_{j-1}(t)\right] = 0,
\end{aligned} \tag{29}$$

where the time step Δt is 0.05.

The initial conditions for this extended traffic lattice model are chosen as follows:

$$\rho_j(1) = \rho_j(0) = \begin{cases} \rho_0, j \neq \dfrac{N}{2}, & \dfrac{N}{2} + 1, \\ \rho_0 - \sigma, & j = \dfrac{N}{2}, \\ \rho_0 + \sigma, & j = \dfrac{N}{2} + 1, \end{cases} \tag{30}$$

where the value of N which defined the sum number of the sites is opted as 100, $a = 1.25$. $\rho_j(0) = \rho_0 = 0.25$, $\rho_j(1) = \rho_0 = 0.25$, for $j \neq 55, 56$, $\rho_j(1) = 0.25 - 0.1$, for $j = 50$, $\rho_j(1) = 0.25 + 0.1$, for $j = 51$, and the value of σ which defined the initial disturbance is opted as 0.05.

Figures 3(a)–3(d) express the three-phase diagram of the new expanded two-lane model under the condition of changing the lane change rate step by step. It shows that when the values of P and β are fixed and unchanged, the vibration amplitude of density wave decreases gradually and the vibration frequency decreases as the value of the lane change rate γ increases from 0 to 0.3. Figure 3(a) reveals when β and P is equal to 0.05 and 0.15, let γ be 0. As can be seen from Figure 3(a) intuitively and effectively, the density wave oscillates, ranging from 0.2 to 0.9, and the vibration frequency is the highest than the other three figures. Figures 3(b) and 3(c) show the phase diagrams at $\gamma = 0.1$ and $\gamma = 0.2$, respectively. When the value of γ is gradually increased to 0.3, the vibration amplitude of density wave is about 0.3 to 0.7 which is shown in Figure 3(d). Through the continuous debugging of numerical simulation, with the gradual increase of γ value, the density wave curve becomes more and more stable. For the actual traffic flow, this means that the traffic operation capacity can be enhanced and the traffic efficiency is greatly improved. Figure 4 is the two-dimensional phase diagrams with density wave corresponding to Figure 3. They finally verify that considering lane change rate is of positive value to traffic flow. Increasing the value of γ in a certain range can improve the ability of traffic flow to run smoothly.

Figures 5(a)–5(d) express the three-dimensional phase diagram of density wave when the values of β and γ are fixed to 0.05 and 0.1, and the values of the coefficient P of the driver's aggressive effect are gradually changed. Figure 5(a) reveals that the curve fluctuation range of density wave ranges from 0.1 to 0.9 without considering the driver's aggressive effect. In Figures 5(b) and 5(c) with the increase of P value to 0.1 and 0.2, the fluctuation range of density wave decreases obviously, and the change of vibration frequency is not significant. When the value of P is increased to 0.3, the density wave presents a straight line, which means that

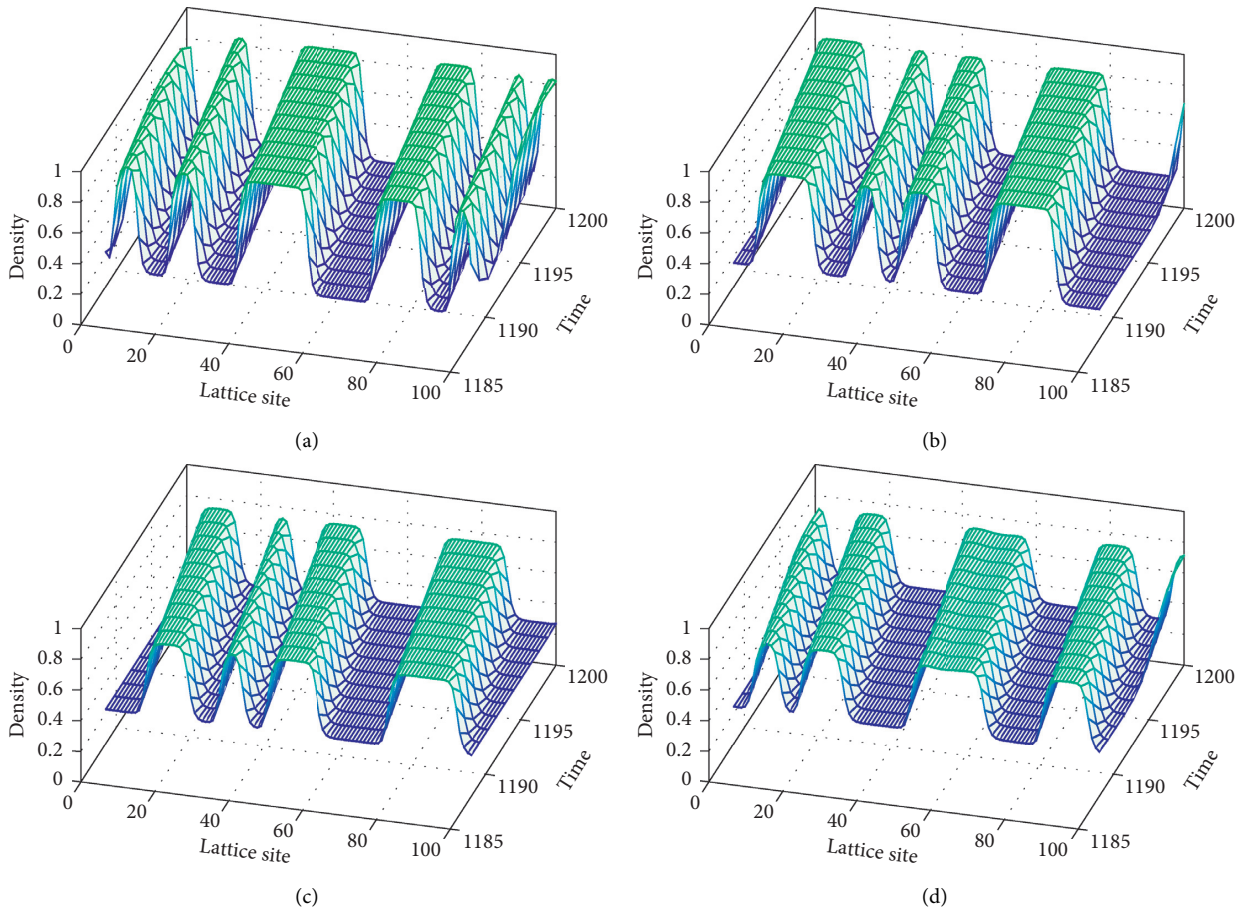

Figure 3: The evolution of the traffic densities with different γ values. (a) $\gamma = 0$. (b) $\gamma = 0.1$. (c) $\gamma = 0.2$. (d) $\gamma = 0.3$.

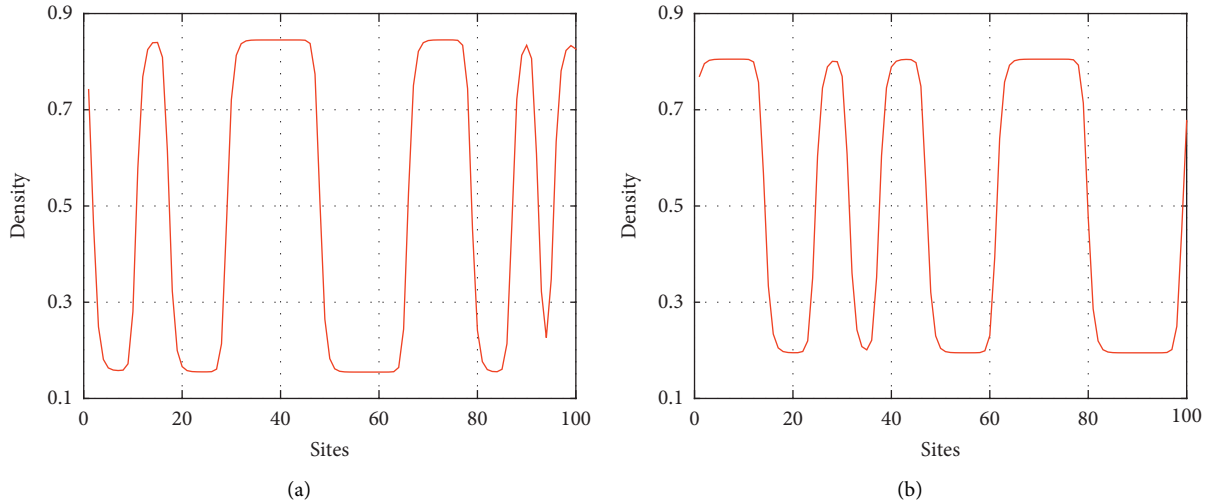

Figure 4: Continued.

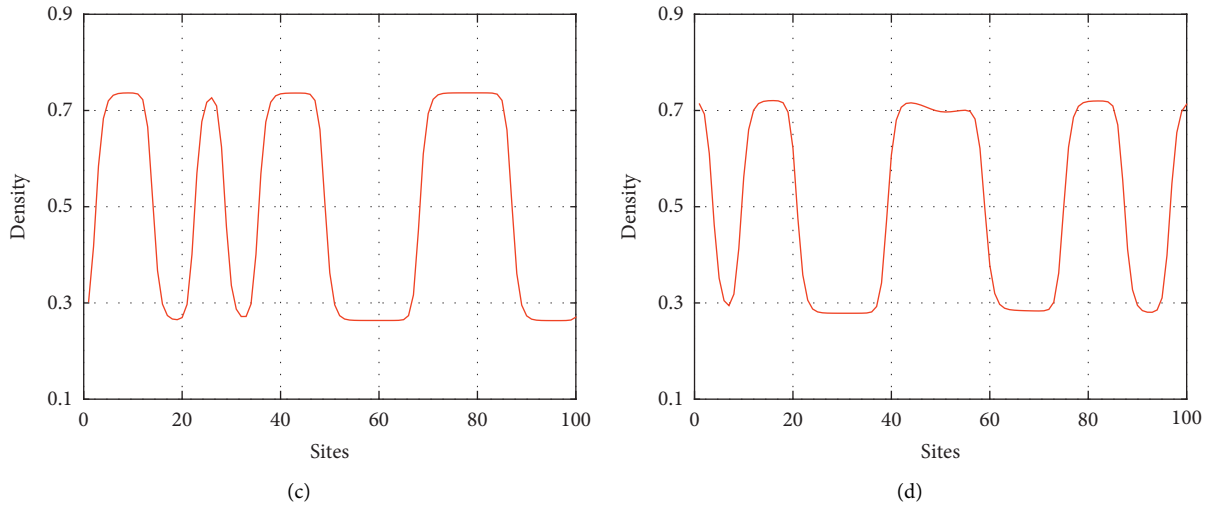

Figure 4: The density profile at $t = 10300$ with different γ values. (a) $\gamma = 0$. (b) $\gamma = 0.1$. (c) $\gamma = 0.2$. (d) $\gamma = 0.3$.

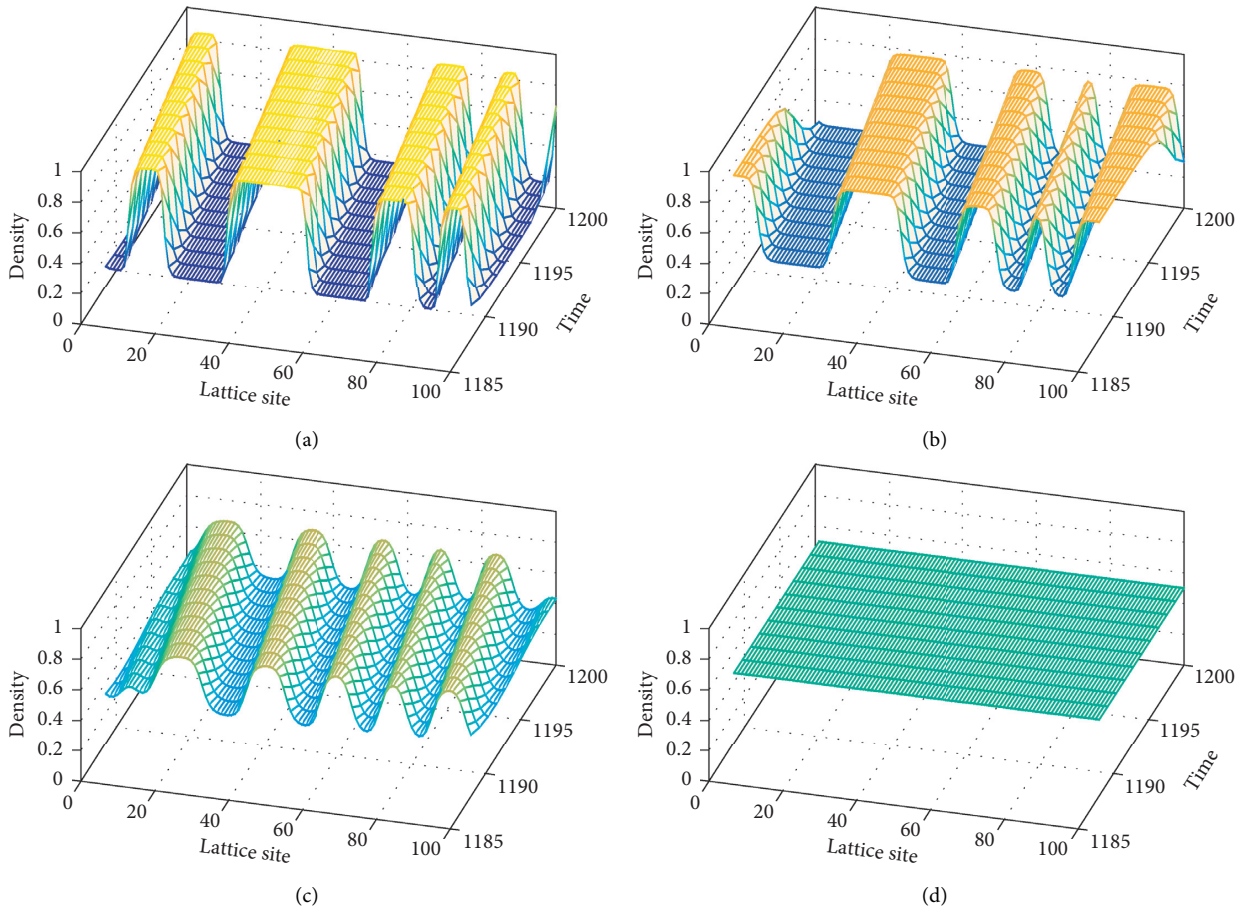

Figure 5: The evolution of the traffic densities with different P values. (a) $P = 0$. (b) $P = 0.1$. (c) $P = 0.2$. (d) $P = 0.3$.

the traffic flow will reach an ideal state without blockage. Figure 6 is the two-dimensional headway profile phase diagram of density wave matching Figure 5. In the two-lane lattice hydrodynamics model, considering the driver's aggressive effect, traffic congestion can be effectively alleviated.

Figures 7 and 8 show the three-dimensional phase diagram and corresponding two-dimensional phase diagram when the value of β is gradually increased from 0 to 0.15 when the values of P and γ are fixed as 0.1 and 0.1. From Figures 7(b)–7(d), with the increase of the influence

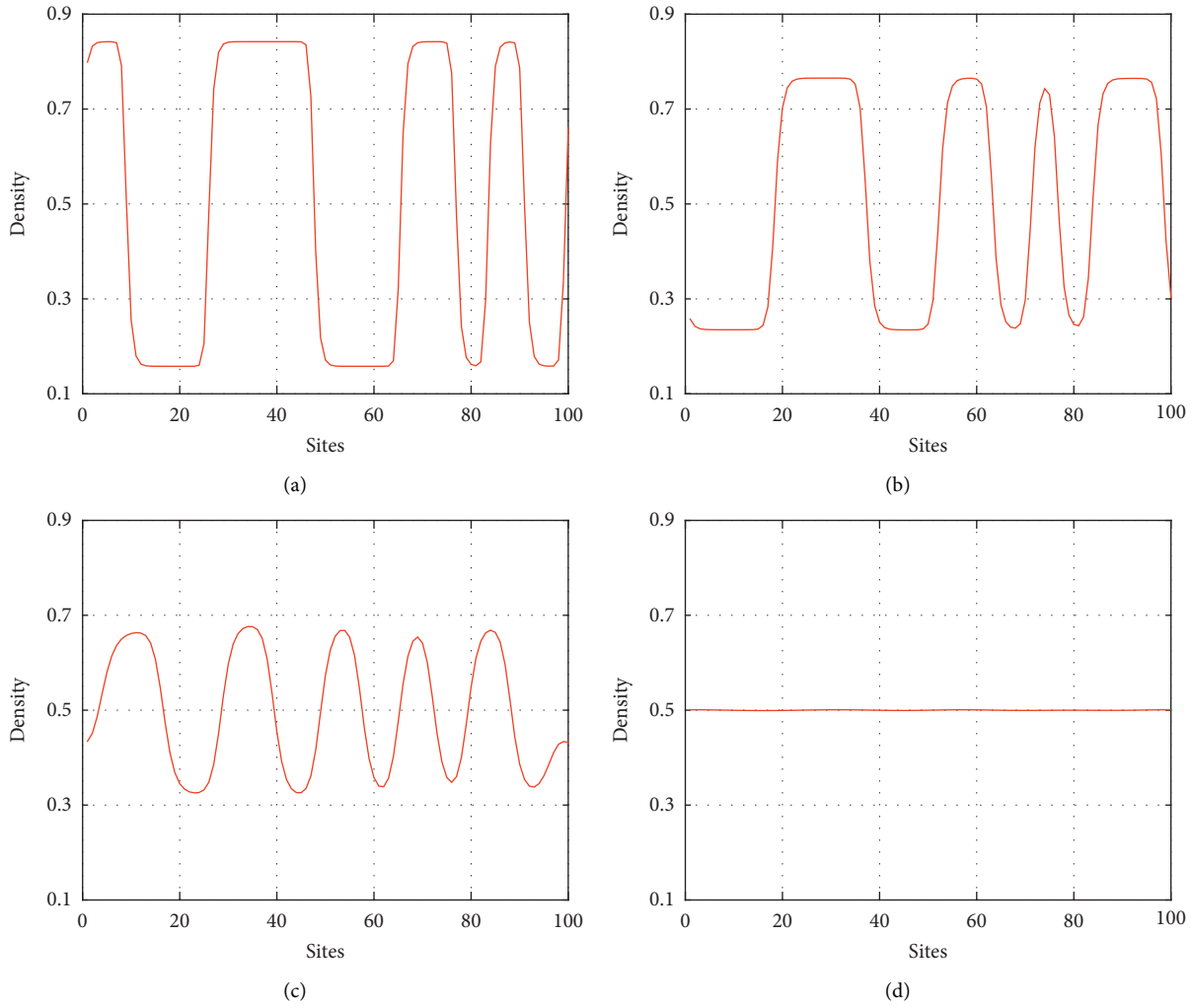

Figure 6: The density profile at $t = 10300$ with different P values. (a) $P = 0$. (b) $P = 0.1$. (c) $P = 0.2$. (d) $P = 0.3$.

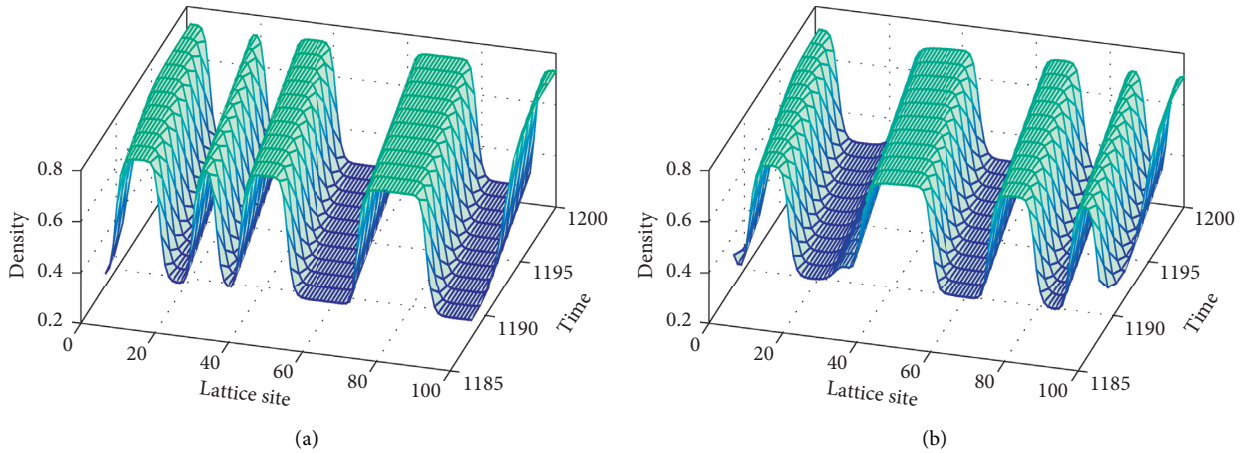

Figure 7: Continued.

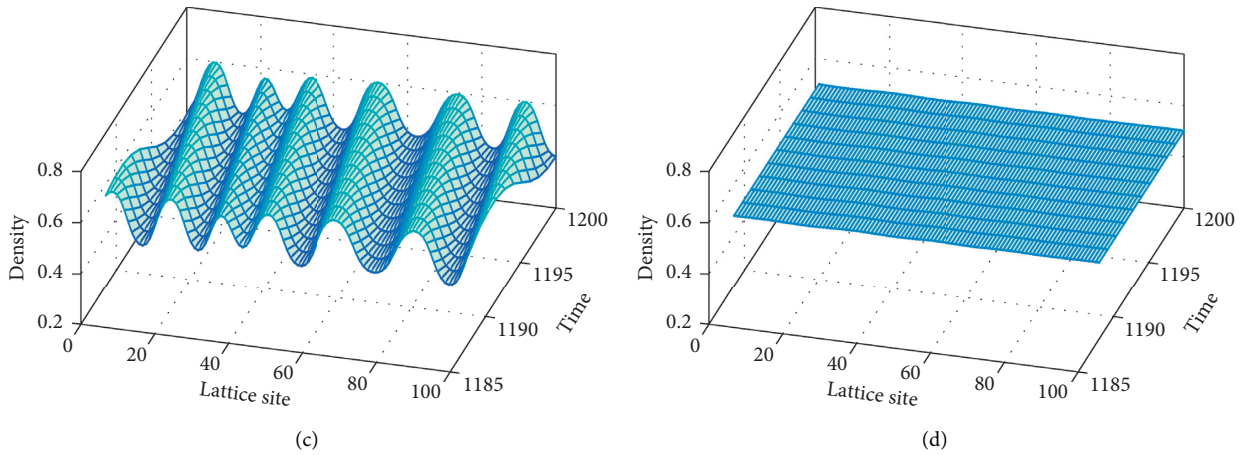

Figure 7: The evolution of the traffic densities with different β values. (a) $\beta = 0$. (b) $\beta = 0.05$. (c) $\beta = 0.1$. (d) $\beta = 0.15$.

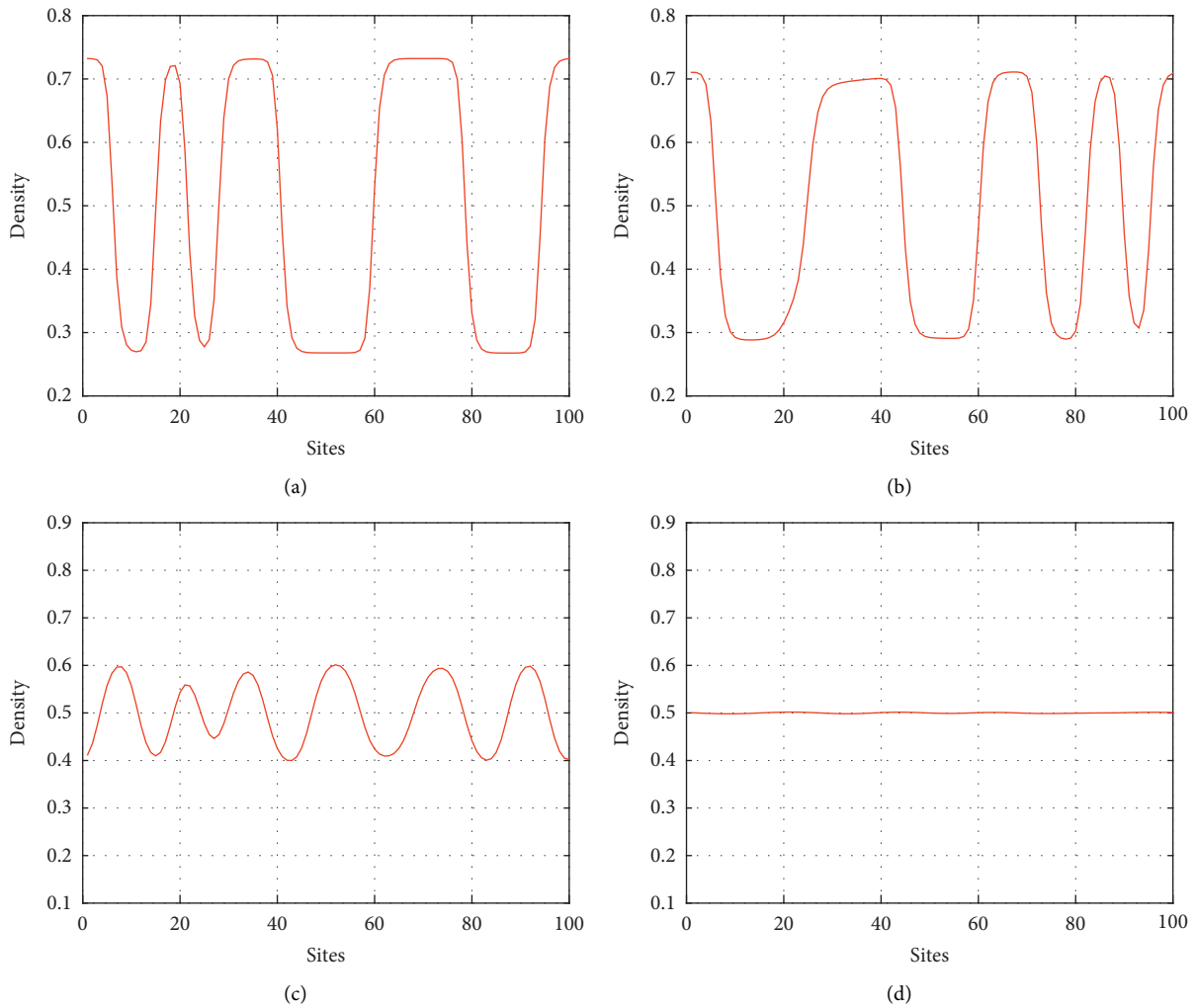

Figure 8: The density profile at $t = 10300$ with different β values. (a) $\beta = 0$. (b) $\beta = 0.05$. (c) $\beta = 0.1$. (d) $\beta = 0.15$.

parameter value β of the relative flow difference integral, the density wave tends to be stable. When the value of β is 0.15, the density wave approximates a straight line. Considering the influence of the relative flow difference integral has a positive effect on traffic flow.

Through numerical simulation, it is proved that considering the factors of the driver's aggressive effect, the relative flow difference integral, and the lane change rate in two-lane traffic flow model is beneficial to improve traffic operation. The numerical simulation results also validate the correctness of our theoretical results in practical operation.

6. Conclusion

According to the actual traffic environment, a novel two-lane lattice hydrodynamic model is proposed, which considers the effects of the driver's aggressive effect and the relative flow difference integral. The analytical stability conditions are obtained by linear stability analysis method, and the spatial phase diagram of sensitivity coefficient density is given. Based on the change of the neutral stability curve in the phase diagram, this paper analyzes the three influencing factors: driver's radical effect, relative flow difference integral, and lane change rate, which play an important role in improving the stability of traffic flow. Nonlinear method is used to analyze the model in advance and the corresponding numerical validation is made. The numerical simulation results are consistent with the theoretical analysis. In conclusion, it is reasonable to consider the driver's aggressive effect and the relative flow difference integral comprehensively in a two-lane lattice hydrodynamic model.

Data Availability

The data used to support the findings of this study are available from the corresponding author upon request.

Conflicts of Interest

The authors declare that there are no conflicts of interest regarding the publication of this paper.

Acknowledgments

This work was supported by the Project of Humanities and Social Science of Education Ministry of China (Grant no. 20YJA630008), the Natural Science Foundation of Zhejiang Province, China (Grant no. LY20G010004), the National Key Research and Development Program of China-Traffic Modeling, Surveillance and Control with Connected & Automated Vehicles (Grant no. 2017YFE9134700), and the K. C. Wong Magna Fund in Ningbo University, China.

References

[1] C. Ma and R. He, "Green wave traffic control system optimization based on adaptive genetic-artificial fish swarm algorithm," *Neural Computing and Applications*, vol. 31, no. 7, pp. 2073–2083, 2019.

[2] C. X. Ma and D. Yang, "Public transit network planning in small cites considering safety and convenience," *Advances in Mechanical Engineering*, vol. 12, pp. 1–12, 2020.

[3] C. X. Ma, W. Hao, F. Q. Pan, and W. Xiang, "Road screening and distribution route multi-objective robust optimization for hazardous materials based on neural network and genetic algorithm," *PLoS One*, vol. 13, no. 6, Article ID e0198931, 2018.

[4] R. Kaur and S. Sharma, "Analysis of driver's characteristics on a curved road in a lattice model," *Physica A: Statistical Mechanics and Its Applications*, vol. 471, pp. 59–67, 2017.

[5] Z. Wang, R. Cheng, and H. Ge, "Nonlinear analysis of an improved continuum model considering mean-field velocity difference," *Physics Letters A*, vol. 383, no. 7, pp. 622–629, 2019.

[6] R. Cheng, H. Ge, and J. Wang, "An extended continuum model accounting for the driver's timid and aggressive attributions," *Physics Letters A*, vol. 381, no. 15, pp. 1302–1312, 2017.

[7] T. Wang, R. Cheng, and H. Ge, "An extended two-lane lattice hydrodynamic model for traffic flow on curved road with passing," *Physica A: Statistical Mechanics and Its Applications*, vol. 533, p. 121915, 2019.

[8] T. Wang, R. Cheng, and H. Ge, "Analysis of a novel two-lane lattice hydrodynamic model considering the empirical lane changing rate and the self-stabilization effect," *IEEE Access*, vol. 7, Article ID 174725, 2019.

[9] Q. T. Zhai, H. X. Ge, and R. J. Cheng, "An extended continuum model considering optimal velocity change with memory and numerical tests," *Physica A*, vol. 490, pp. 774–785, 2018.

[10] T.-Q. Tang, W.-F. Shi, H.-J. Huang, W.-X. Wu, and Z. Song, "A route-based traffic flow model accounting for interruption factors," *Physica A: Statistical Mechanics and Its Applications*, vol. 514, pp. 767–785, 2019.

[11] R. J. Cheng, H. X. Ge, and J. F. Wang, "The nonlinear analysis for a new continuum model considering anticipation and traffic jerk effect," *Applied Mathematics and Computation*, vol. 332, pp. 493–505, 2018.

[12] T. Nagatani, "Modified KdV equation for jamming transition in the continuum models of traffic," *Physica A*, vol. 261, no. 3-4, pp. 599–607, 1998.

[13] T. Nagatani, "TDGL and MKdV equations for jamming transition in the lattice models of traffic," *Physica A: Statistical Mechanics and Its Applications*, vol. 264, no. 3-4, pp. 581–592, 1999.

[14] Y. Xue, "Lattice models of the optimal traffic current," *Acta Physica Sinica*, vol. 53, pp. 25–30, 2004.

[15] H. X. Ge, S. Q. Dai, Y. Xue, and L. Y. Dong, "Stabilization analysis and modified Korteweg-de Vries equation in a cooperative driving system," *Physical Review E*, vol. 71, Article ID 066119, 2005.

[16] H.-X. Ge and R.-J. Cheng, "The "backward looking" effect in the lattice hydrodynamic model," *Physica A: Statistical Mechanics and Its Applications*, vol. 387, no. 28, pp. 6952–6958, 2008.

[17] W. X. Zhu, "A backward looking optimal current lattice model," *Communications in Theoretical Physics*, vol. 50, pp. 753–756, 2008.

[18] W.-X. Zhu and E.-X. Chi, "Analysis of generalized optimal current lattice model for traffic flow," *International Journal of Modern Physics C*, vol. 19, no. 5, pp. 727–739, 2008.

[19] G. Peng, W. Lu, and H. He, "Impact of the traffic interruption probability of optimal current on traffic congestion in lattice

model," *Physica A: Statistical Mechanics and Its Applications*, vol. 425, pp. 27–33, 2015.

[20] G. Peng, F. Nie, B. Cao, and C. Liu, "A driver's memory lattice model of traffic flow and its numerical simulation," *Nonlinear Dynamics*, vol. 67, no. 3, pp. 1811–1815, 2012.

[21] J. F. Tian, B. Jia, X. G. Li, and Z. Y. Gao, "Flow difference effect in the lattice hydrodynamic model," *Chinese Physics B*, vol. 19, no. 4, Article ID 040303, 2010.

[22] J. F. Tian, Z. Z. Yuan, B. Jia, M. H. Li, and G. J. Jiang, "The stabilization effect of the density difference in the modified lattice hydrodynamic model of traffic flow," *Physica A*, vol. 391, no. 19, pp. 4476–4482, 2010.

[23] R. Cheng, F. Liu, and H. Ge, "A new continuum model based on full velocity difference model considering traffic jerk effect," *Nonlinear Dynamics*, vol. 89, no. 1, pp. 639–649, 2017.

[24] R. Jiang, Q.-S. Wu, and Z.-J. Zhu, "A new continuum model for traffic flow and numerical tests," *Transportation Research Part B: Methodological*, vol. 36, no. 5, pp. 405–419, 2002.

[25] X. Wu, X. Zhao, H. Song, Q. Xin, and S. Yu, "Effects of the prevision relative velocity on traffic dynamics in the ACC strategy," *Physica A: Statistical Mechanics and Its Applications*, vol. 515, pp. 192–198, 2019.

[26] C. T. Jiang, H. X. Ge, and R. J. Cheng, "Mean-field flow difference model with consideration of on-ramp and off-ramp," *Physica A*, vol. 513, pp. 465–467, 2019.

[27] A. B. Kiselev, V. F. Nikitin, N. N. Smirnov, and M. V. Yumashev, "Irregular traffic flow on a ring road," *Journal of Applied Mathematics and Mechanics*, vol. 64, no. 4, pp. 627–634, 2000.

[28] T.-Q. Tang, X.-F. Luo, J. Zhang, and L. Chen, "Modeling electric bicycle's lane-changing and retrograde behaviors," *Physica A: Statistical Mechanics and Its Applications*, vol. 490, pp. 1377–1386, 2018.

[29] F. Lv, H.-B. Zhu, and H.-X. Ge, "TDGL and mKdV equations for car-following model considering driver's anticipation," *Nonlinear Dynamics*, vol. 77, no. 4, pp. 1245–1250, 2014.

[30] R. Cheng and Y. Wang, "An extended lattice hydrodynamic model considering the delayed feedback control on a curved road," *Physica A: Statistical Mechanics and Its Applications*, vol. 513, pp. 510–517, 2019.

[31] G. Peng, W. Lu, H. He, and Z. Gu, "Nonlinear analysis of a new car-following model accounting for the optimal velocity changes with memory," *Communications in Nonlinear Science and Numerical Simulation*, vol. 40, pp. 197–205, 2016.

[32] Y. Sun, H. Ge, and R. Cheng, "An extended car-following model considering driver's memory and average speed of preceding vehicles with control strategy," *Physica A: Statistical Mechanics and Its Applications*, vol. 521, pp. 752–761, 2019.

[33] H. Song, H. Ge, F. Chen, and R. Cheng, "TDGL and mKdV equations for car-following model considering traffic jerk and velocity difference," *Nonlinear Dynamics*, vol. 87, no. 3, pp. 1809–1817, 2017.

[34] W.-X. Zhu and H. M. Zhang, "Analysis of mixed traffic flow with human-driving and autonomous cars based on car-following model," *Physica A: Statistical Mechanics and Its Applications*, vol. 496, pp. 274–285, 2018.

[35] H. Ou and T.-Q. Tang, "An extended two-lane car-following model accounting for inter-vehicle communication," *Physica A: Statistical Mechanics and Its Applications*, vol. 495, no. 1, pp. 260–268, 2018.

[36] T.-Q. Tang, Y.-X. Rui, J. Zhang, and H.-Y. Shang, "A cellular automation model accounting for bicycle's group behavior," *Physica A: Statistical Mechanics and Its Applications*, vol. 492, pp. 1782–1797, 2018.

[37] K. Nagel and M. Schreckenberg, "A cellular automaton model for freeway traffic," *Journal De Physique I*, vol. 2, pp. 212–229, 1992.

[38] N. Moussa and A. K. Daoudia, "Numerical study of two classes of cellular automaton models for traffic flow on a two-lane roadway," *The European Physical Journal B—Condensed Matter*, vol. 31, no. 3, pp. 413–420, 2003.

[39] S. Das, "Cellular automata based traffic model that allows the cars to move with a small velocity during congestion," *Chaos, Solitons & Fractals*, vol. 44, no. 4-5, pp. 185–190, 2011.

[40] T. Chmura, B. Herz, F. Knorr, T. Pitz, and M. Schreckenberg, "A simple stochastic cellular automaton for synchronized traffic flow," *Physica A: Statistical Mechanics and Its Applications*, vol. 405, pp. 332–337, 2014.

[41] S. Q. Xue, B. Jia, and R. Jiang, "A behaviour based cellular automaton model for pedestrian counter flow," *Journal of Statistical Mechanics: Theory and Experiment*, vol. 2016, no. 11, pp. 1742–5468, 2016.

[42] R. Cheng, H. Ge, and J. Wang, "An extended macro traffic flow model accounting for multiple optimal velocity functions with different probabilities," *Physics Letters A*, vol. 381, no. 32, pp. 2608–2620, 2017.

[43] G. H. Peng, W. Song, Y. J. Peng, and S. H. Wang, "A novel macro model of traffic flow with the consideration of anticipation optimal velocity," *Physica A: Statistical Mechanics and Its Applications*, vol. 398, pp. 76–82, 2014.

[44] T.-Q. Tang, H.-J. Huang, and H.-Y. Shang, "An extended macro traffic flow model accounting for the driver's bounded rationality and numerical tests," *Physica A: Statistical Mechanics and Its Applications*, vol. 468, pp. 322–333, 2017.

[45] R. Mohan and G. Ramadurai, "Heterogeneous traffic flow modelling using second-order macroscopic continuum model," *Physics Letters A*, vol. 381, no. 3, pp. 115–123, 2017.

[46] P. Goatin and F. Rossi, "A traffic flow model with non-smooth metric interaction: well-posedness and micro-macro limit," *Communications in Mathematical Sciences*, vol. 15, no. 1, pp. 261–287, 2017.

[47] T. Q. Tang, H. J. Huang, S. C. Wong, Z. Y. Gao, and Y. Zhang, "A new macro model for traffic flow on a highway with ramps and numerical tests," *Communications in Theoretical Physics*, vol. 51, pp. 71–78, 2009.

[48] G. Peng, "A new lattice model of traffic flow with the consideration of individual difference of anticipation driving behavior," *Communications In Nonlinear Science and Numerical Simulation*, vol. 18, no. 10, pp. 2801–2806, 2013.

[49] G. H. Peng, X. H. Cai, C. Q. Liu, and B. F. Cao, "A new lattice model of traffic flow with the consideration of the driver's forecast effects," *Physics Letters A*, vol. 375, no. 22, pp. 2153–2157, 2011.

[50] G. H. Peng, X. H. Cai, C. Q. Liu, and M. X. Tuo, "A new lattice model of traffic flow with the anticipation effect of potential lane changing," *Physics Letters A*, vol. 376, no. 4, pp. 447–451, 2012.

[51] H.-X. Ge, P.-J. Zheng, S.-M. Lo, and R.-J. Cheng, "TDGL equation in lattice hydrodynamic model considering driver's physical delay," *Nonlinear Dynamics*, vol. 76, no. 1, pp. 441–445, 2014.

[52] A. K. Gupta, S. Sharma, and P. Redhu, "Effect of multi-phase optimal velocity function on jamming transition in a lattice hydrodynamic model with passing," *Nonlinear Dynamics*, vol. 80, no. 3, pp. 1091–1108, 2015.

[53] T. Nagatani, "Dynamical jamming transition induced by a car accident in traffic-flow model of a two-lane roadway," *Physica*

A: Statistical Mechanics and Its Applications, vol. 202, no. 3-4, pp. 449–458, 1994.

[54] T. Nagatani, "Self-organization and phase transition in traffic-flow model of a two-lane roadway," *Journal of Physics A: Mathematical and General*, vol. 26, no. 17, pp. L781–L787, 1999.

[55] G. Peng, S. Yang, D. Xia, and X. Li, "A novel lattice hydrodynamic model considering the optimal estimation of flux difference effect on two-lane highway," *Physica A: Statistical Mechanics and Its Applications*, vol. 506, pp. 929–937, 2018.

[56] J. He, H. Yang, H.-J. Huang, and T.-Q. Tang, "Impacts of wireless charging lanes on travel time and energy consumption in a two-lane road system," *Physica A: Statistical Mechanics and Its Applications*, vol. 500, pp. 1–10, 2018.

[57] X. Li, K. Fang, and G. Peng, "A new lattice model accounting for multiple optimal current differences' anticipation effect in two-lane system," *Physica A: Statistical Mechanics and Its Applications*, vol. 486, pp. 814–826, 2017.

[58] T. Wang, J. Zhang, Z. Gao, W. Zhang, and S. Li, "Congested traffic patterns of two-lane lattice hydrodynamic model with on-ramp," *Nonlinear Dynamics*, vol. 88, no. 2, pp. 1345–1359, 2017.

[59] W. Knospe, L. Santen, A. Schadschneider, and M. Schreckenberg, "A realistic two-lane traffic model for highway traffic," *Journal of Physics A: Mathematical and General*, vol. 35, no. 15, pp. 3369–3388, 2002.

[60] R. Kaur and S. Sharma, "Modeling and simulation of driver's anticipation effect in a two-lane system on curved road with slope," *Physica A: Statistical Mechanics and Its Applications*, vol. 499, pp. 110–120, 2018.

[61] F. Sun, A. H. F. Chow, S. M. Lo, and H. Ge, "A two-lane lattice hydrodynamic model with heterogeneous lane changing rates," *Physica A: Statistical Mechanics and Its Applications*, vol. 511, pp. 389–400, 2018.

[62] H.-d. He, C.-y. Zhang, W.-l. Wang, Y.-y. Hao, and Y. Ding, "Feedback control scheme for traffic jam and energy consumption based on two-lane traffic flow model," *Transportation Research Part D: Transport and Environment*, vol. 60, pp. 76–84, 2018.

[63] X.-G. Li, B. Jia, Z.-Y. Gao, and R. Jiang, "A realistic two-lane cellular automata traffic model considering aggressive lane-changing behavior of fast vehicle," *Physica A: Statistical Mechanics and Its Applications*, vol. 367, pp. 479–486, 2006.

[64] F. Liu and Y. Cheng, "The improved element-free galerkin method based on the nonsingular weight functions for inhomogeneous swelling of polymer gels," *International Journal of Applied Mechanics*, vol. 10, no. 4, Article ID 1850047, 2018.

[65] F. Liu, Q. Wu, and Y. Cheng, "A meshless method based on the nonsingular weight functions for elastoplastic large deformation problems," *International Journal of Applied Mechanics*, vol. 11, no. 1, Article ID 1950006, 2019.

[66] J. Wang and F. Sun, "A hybrid variational multiscale element-free galerkin method for convection-diffusion problems," *International Journal of Applied Mechanics*, vol. 11, no. 07, Article ID 1950063, 2019.